Theory of electronic and optical properties of 3C-SiC

George Theodorou[a] and George Tsegas
Department of Physics, Aristotle University of Thessaloniki, 540 06 Thessaloniki, Greece

Efthimios Kaxiras[b]
Department of Physics, University of Crete, Heraklion 71102, Greece

(Received 21 September 1998; accepted for publication 16 November 1998)

We study the electronic and optical properties of cubic (3C) SiC, using a combination of first-principles and tight-binding electronic structure calculations. We employ pseudopotential density functional theory calculations, with appropriate corrections to the energy of conduction bands, to investigate the band structure of this material and obtain band gaps that are in agreement with experimental results. The optical properties are then studied within the framework of the empirical tight-binding model, which is fitted to reproduce the first-principles calculations. This approach allows for a thorough investigation of the dielectric functions, the reflectivity, and the refractive index. Critical points are identified and connected to the appropriate transitions in the band structure. The results are in good agreement with available experimental data. In addition, we investigate spin splitting effects. © *1999 American Institute of Physics.* [S0021-8979(99)05604-2]

I. INTRODUCTION

Silicon carbide possesses a number of unique properties which make it a potential candidate for semiconducting device applications.[1,2] Its high bond energy (~ 5 eV) makes SiC resistant to high temperature and radiation and is responsible for its hardness, chemical inertness, and low diffusion rates of dopants and host atoms. A comparison with other semiconducting materials, such as GaAs and GaP, reveals certain advantages for SiC devices: high operating temperature, an order of magnitude higher avalanche breakdown field, high thermal conductivity (close to that of copper), and higher saturation value of electron drift velocity, which can lead to higher output power as well as operating frequency. In addition, the wide gap of this material suggests that it would be feasible to construct light-emitting diodes operational in the entire visible spectrum and the ultraviolet region.

Experimental progress in the study of SiC has been obstructed for many years by the difficulty of growing homogeneous single crystals, partly because of the large number of SiC polytypes. Recent developments on bulk crystal growth[3] and control of polytypism[4] in epitaxially grown layers, have yielded high quality single crystals, making possible the systematic experimental study of this material. These studies include reports on reflectivity,[5–7] electroreflectivity,[8] and spectroscopic ellipsometry[9–11] mainly on 3C-SiC, the cubic form of SiC. This material, on which the present work will be focused, is the only IV–IV compound with zinc-blende structure that exists in nature.

First-principles calculations have already been reported for the electronic properties of 3C-SiC. Using the GW approximation (where the self-energy operator is given as a product of the Green's function G times the screened Coulomb interaction W), Rohlfing, Krüger, and Pollman[12] calculated the band structure of 3C-SiC; Willatzen, Cardona, and Christensen,[13] using the linear muffin-tin orbital method (LMTO), calculated effective masses, Luttinger parameters, and spin splitting effects of zinc-blende type SiC. First-principles methods have also been applied to investigate optical properties.[6,14–19] The first-principles calculations of optical response is time consuming and can be carried out only with a small number of **k** points in the full Brillouin Zone (BZ). Consequently, investigation of the optical properties with a computational efficient scheme is desirable; such a scheme is the empirical tight-binding (ETB) method. In the present work, we use a tight-binding model[20] with a sp^3 set of orbitals and second nearest neighbor interactions for the study of the electronic and optical properties of 3C-SiC. The interaction parameters needed in the ETB scheme are obtained by fitting the band structure of the material as obtained from first-principles calculations based on the density functional theory and pseudopotentials. With these parameters as input to our ETB model, we are able to calculate the dielectric function, the refractive index, and the reflectivity of 3C-SiC, using large sets of **k** points to obtain well converged results.

The remainder of the article is organized as follows: Section II describes the computational approaches for band structure calculations, Sec. III discusses the optical properties, Sec. IV presents the details of the spin splittings, and Sec. V gives our conclusions.

II. COMPUTATIONAL APPROACHES

A. First-principles calculations

We use Density Functional Theory in the local density approximation (DFT-LDA)[21] to obtain a self-consistent solution for the valence electrons in bulk phases of SiC, at various lattice constants and under certain deformations (see de-

[a]Electronic mail: theodoru@ccf.auth.gr
[b]On leave of absence from Department of Physics and Division of Applied Sciences, Harvard University, Cambridge, MA 02138.

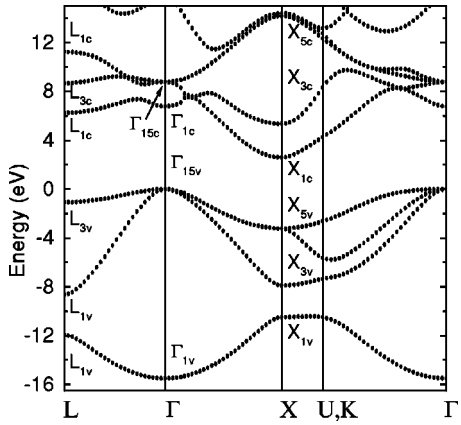

FIG. 1. Band structure for 3C-SiC, calculated using the DFT-LDA method, without spin–orbit coupling.

tails below). The atomic cores are represented by nonlocal norm-conserving pseudopotentials from Bachelet, Hamann, and Schlüter.[22] We use plane waves with a cutoff of 48 Ry to expand the wave functions and the potentials and a grid of $6\times6\times6$ **k** points of the Monkhorst–Pack type[23] in the full BZ. These computational parameters give well converged results for the total energy and the band structure of this system. For example, the calculated lattice constant and bulk modulus are 4.33 Å, and 223 GPa, respectively, in excellent agreement with the corresponding experimental values of 4.3596 Å and 224 GPa, respectively.

As is well known, the energies of conduction states are not well reproduced by the DFT-LDA approach.[24] For this reason, we have used the recently introduced, by Fritsche and co-workers,[25] Generalized Density Functional Theory (GDFT) correction to DFT/LDA eigenvalues, for the evaluation of the energy band states. A thorough study of the ability of the GDFT has been undertaken by Remediakis and Kaxiras.[26] Their work shows that this theory gives reasonably accurate results for the band gap of many semiconductor compounds containing elements from the second to fourth rows of the periodic table (to about 10% of the experimental values or better). Based on this work, we suggest that the results of the present work which includes the GDFT correction to DFT/LDA eigenvalues are accurate and reliable. which we find to work rather satisfactorily, at least for the system under consideration. The band structure from the DFT/LDA calculations is shown in Fig. 1. Selected energy eigenvalues at various high symmetry points of the BZ are listed in Table I, along with the results of the GW method.[12] In both cases, spin–orbit coupling has not been taken into account. We also include experimental data in Table I, for comparison to the theoretical results. The agreement between the present calculations, the GW results, and the experimental data is excellent, including the value for the fundamental gap.

A useful quantity to examine in studying electronic structure is how the presence of strain in the crystal changes the band energies. The change in the energy eigenvalues at specific symmetry points is described in terms of the deformation potentials. In the present work we investigate the deformation potentials for the band maxima and minima at

TABLE I. Eigenvalues (in electron volts) at high-symmetry points of the BZ. In the first column are results from the present DFT-LDA method, in the second from the GW method (Ref. 12), in the third from the present ETB model, and in the fourth experimental data. All calculation are done without spin–orbit coupling.

	DFT-LDA	GW (Ref. 12)	ETB	Expt.
Γ_{1v}	−15.51	−16.54	−15.04	⋯
Γ_{15v}	0.0	0.0	0.0	0.0
Γ_{1c}	6.77	7.24	7.07	7.4[a]
Γ_{15c}	8.77	8.35	8.98	7.75,[b] 9.0±0.2[c]
X_{1v}	−10.50	−11.46	−10.18	⋯
X_3^v	−7.89	−8.65	−7.59	⋯
X_{5v}	−3.24	−3.65	−3.20	−3.6,[b] −3.4[a]
X_{1c}	2.59	2.18	2.47	2.39[b]
X_{3c}	5.34	5.48	5.64	5.5,[b] 4.7[b]
X_{5c}	14.17	15.91	13.50	⋯
L_{1v}	−11.95	−12.93	−11.99	⋯
L_{1v}	−8.63	−9.43	−8.65	⋯
L_{3v}	−1.08	−1.22	−1.18	−1.16[b]
L_{1c}	6.24	6.46	6.22	⋯
L_{3c}	8.65	8.52	9.11	8.5[b]
L_{1c}	11.23	11.97	11.53	⋯
$E_{\text{gap}}^{\text{ind}}$	2.59	2.18	2.47	2.39,[b] 2.416[b]

[a]From Ref. 6.
[b]From Ref. 27.
[c]From Ref. 7.

the Γ point of the BZ. The strain under consideration has two components, a hydrostatic and a uniaxial one. In the absence of spin–orbit coupling, the change in energy at the top of the valence band under hydrostatic and uniaxial pressure along the [001] direction is given by[28]

$$\delta E_{hh}=\delta E_h^v+\delta E_{001}, \tag{1}$$

$$\delta E_{lh}=\delta E_h^v-(\tfrac{1}{2})\,\delta E_{001}, \tag{2}$$

$$\delta E_{sh}=\delta E_h^v-(\tfrac{1}{2})\,\delta E_{001}, \tag{3}$$

with $\delta E_h=a^v Tr[\epsilon]$, $\delta E_{001}=2b(\epsilon_{zz}-\epsilon_{xx})$, and $[\epsilon]$ the strain tensor, while the change at the lowest conduction band under hydrostatic pressure is given by

$$\delta E_c=\delta E_h^c, \tag{4}$$

with $\delta E_h^c=a^c Tr[\epsilon]$. The variation of the energy values with strain was calculated with the use of the DFT-LDA method; the obtained values for the deformation potentials $a=a^c-a^v$ and b are

$$a=-9.8\ \text{eV} \quad \text{and} \quad b=-3.8\ \text{eV}. \tag{5}$$

B. Empirical tight binding method

The second approach utilized in the present article is the ETB method.[20,29,30] The calculations are based on an ETB model Hamiltonian, in the three-center representation, with an orthogonal sp^3 set of orbitals and interactions up to second neighbor. The values of the interaction parameters are determined by fitting the band structure results from the DFT-LDA calculations discussed above. The interaction parameters so obtained are listed in Table II. Note that in the fitting process the calculations with the ETB model were done without taking into account spin–orbit coupling as in

TABLE II. Interaction parameters (in electron volts) for 3C-SiC in the ETB model. The notation is that of Slater–Koster.

E^c_{ss}	1.3903	$E^c_{ss}(0.5,0.5,0.0)$	0.3828
E^c_{pp}	4.8964	$E^c_{sx}(0.0,0.5,0.5)$	−0.6001
E^a_{ss}	−10.1321	$E^c_{sx}(0.5,0.5,0.0)$	−0.0496
E^a_{pp}	2.3355	$E^c_{xx}(0.5,0.5,0.0)$	0.4746
		$E^c_{xx}(0.0,0.5,0.5)$	0.0124
$E_{ss}(0.25,0.25,0.25)$	−1.1961	$E^c_{xy}(0.5,0.5,0.0)$	0.1612
$E_{sx}(0.25,0.25,0.25)$	0.9683	$E^c_{xy}(0.0,0.5,0.5)$	0.1392
$E_{xs}(0.25,0.25,0.25)$	−1.6405	$E^a_{ss}(0.5,0.5,0.0)$	−0.3185
$E_{xx}(0.25,0.25,0.25)$	0.3621	$E^a_{sx}(0.0,0.5,0.5)$	−0.4360
$E_{xy}(0.25,0.25,0.25)$	2.0866	$E^a_{sx}(0.5,0.5,0.0)$	−0.6421
		$E^a_{xx}(0.5,0.5,0.0)$	0.1278
		$E^a_{xx}(0.0,0.5,0.5)$	−0.7800
		$E^a_{xy}(0.5,0.5,0.0)$	0.0118
		$E^a_{xy}(0.0,0.5,0.5)$	−0.3843

the DFT-LDA calculations. Utilizing this set of interaction parameters, energy eigenvalues at various high symmetry points of the BZ were calculated and the results are listed in Table I, along with the results from our DFT-LDA calculations and those of a GW calculation,[12] and experimental data. The band structure from the ETB calculations for 3C-SiC is shown in Fig. 2. From Fig. 2 and Table I, we conclude that the ETB model describes very well not only the valence bands but also the lowest conduction bands. For a more detailed comparison, we present in Table III the calculated values of direct gaps in 3C-SiC and the experimental results, which are in good agreement.

III. OPTICAL PROPERTIES

Having established an ETB model which successfully accounts for the band structure of 3C-SiC, we proceed with the calculation of the optical properties of the material. In all subsequent calculations of the present work spin–orbit coupling, thus far ignored, will be incorporated. The spin–orbit coupling is discussed in detail Sec. IV. For the calculation of the imaginary part, $\varepsilon_2(\omega)$, of the dielectric function we use the expression[31]

TABLE III. Direct gaps (in electron volts) for 3C-SiC, calculated within the ETB model. Experimental results are also included.

	Theory	Expt. (Ref. 7)
$\Gamma_{1c}-\Gamma_{15v}$	7.07	7.4
$L_{1c}-L_{3v}$	7.40	7.5
$X_{3c}-X_{5v}$	5.67	5.8
$\Gamma_{15c}-\Gamma_{15v}$	8.98	9.0

$$\varepsilon_2(\omega)=\frac{4\pi^2e^2}{m^2\omega^2}\sum_{c,v}\int\frac{2}{(2\pi)^3}|\langle\mathbf{k},c|\mathbf{P}\cdot\mathbf{a}|\mathbf{k},v\rangle|^2 \times\delta[E_{cv}(\mathbf{k})-\hbar\omega]d\mathbf{k}, \tag{6}$$

where $|\mathbf{k},c\rangle$ and $|\mathbf{k},v\rangle$ stand for the wave functions of the conduction and the valence bands, respectively, and $E_{cv}(\mathbf{k})$ for the energy difference between the c-conduction and the v-valence band. **P** is the momentum operator and **a** the polarization unit vector. In our ETB scheme the momentum matrix elements are expressed in terms of the Hamiltonian matrix elements and distances between localized orbitals.[32,33,29] The integration in the BZ is performed within the linear analytic tetrahedron method[34,35] by using a uniform mesh of $40\times40\times40$ **k** points. The real part of the dielectric function, $\varepsilon(\omega)$, is obtained by a Kramers–Kronig analysis.

Figure 3 shows the calculated real and imaginary part of the dielectric function for 3C-SiC and Fig. 4 the second derivative of the dielectric function with respect to energy. The calculated dielectric function exhibits a number of critical points. The lowest one at 5.7 eV comes from direct transitions between the highest valence and lowest conduction band in the vicinity of the minimum direct gap, located along the Δ direction and close to the X point. The critical point at 7.5 eV is connected to transitions between the highest valence and lowest conduction band along the Λ line. A set of three critical points at 7.8, 8.0, and 8.2 eV are connected to transitions between the highest valence and lowest conduction band in a region around the ΓK line and an extended region in the ΓXUL plane. A point at 8.95 eV is connected

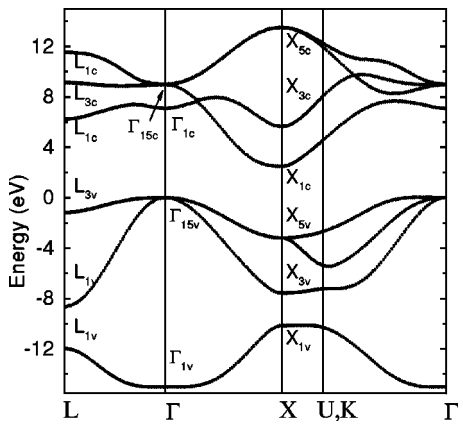

FIG. 2. Band structure for 3C-SiC, calculated using the ETB method, without spin–orbit coupling.

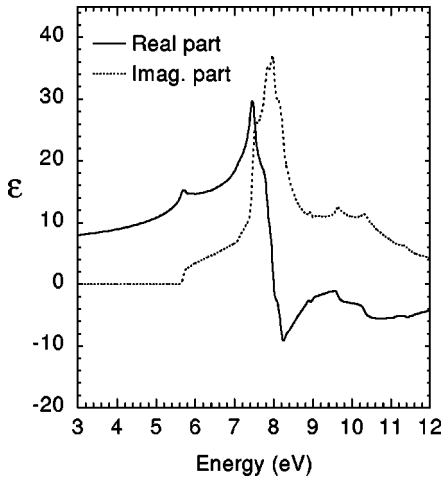

FIG. 3. Calculated real and imaginary part of the dielectric function for 3C-SiC.

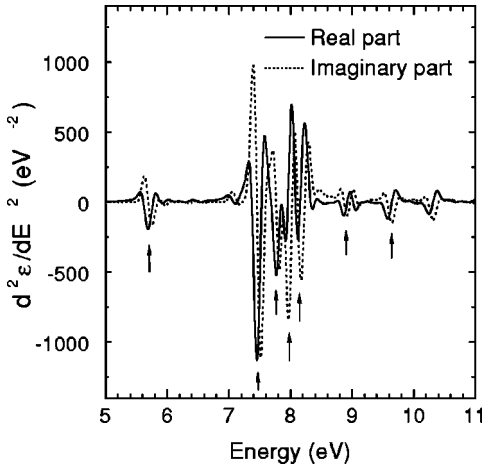

FIG. 4. Calculated second derivative, $d^2\varepsilon/dE^2$, of the dielectric function with respect to energy for 3C-SiC.

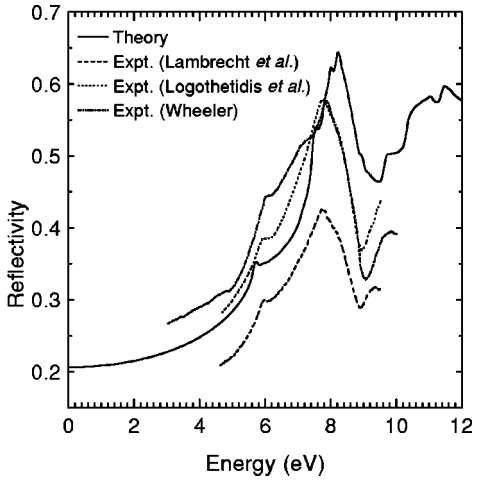

FIG. 5. Calculated reflectivity for normal incidence for 3C-SiC. We also include the experimental data of Lambrect *et al.* (Ref. 6), Logothetidis *et al.* (Ref. 10), and Wheeler (Ref. 5).

to transitions between the highest valence and second lowest conduction band along the Λ line and close to the Γ point. Finally, one point at 9.6 eV is related to transitions between the highest valence and second lowest conduction band along the Δ line and near the X point.

Experimental results from Ref. 9 reveal a group of critical points located at 6.4, 7.0, 7.3, and 7.7 eV. The structure around these critical points is similar to that found in our calculations for the critical points located at 7.5, 7.8, 8.0, and 8.2 eV, despite the fact that the calculated critical points occur at higher energies. Recent experimental results of Ref. 11 have shown critical points at the energies of 5.96, 7.43, 7.73, 9.03, and 9.4 eV. The correspondence between the experimental and calculated critical points is the following: The experimental critical point at 5.96 eV corresponds to the calculated at one 5.7 eV; the 7.43 eV (experiment) to 7.5 eV (theory), the 7.73 eV (experiment) to 7.8 eV (theory), the 9.03 eV (experiment) to 8.95 eV (theory), and the 9.49 eV (experiment) to 9.6 eV (theory). Also it should be noted that experimental results are quite sensitive to the quality of the surface. Roughness at the surface diffuses light, and the presence of surface oxide also affects the intensity of the recorded reflected light. These effects become stronger at higher energies. In addition, samples might contain different SiC polytypes. Finally, life-time broadening smears out the critical point structures. All these effects influence the experimental results.

The calculated value of the static dielectric constant, corresponding to ε_∞, is 7.1 and is listed along with experimental and theoretical results in Table IV. This value is slightly larger than the experimental values. In Fig. 5 we present the results for the calculated reflectivity for normal incidence, which also exhibits the same critical points as the dielectric function. In Fig. 5, experimental results for reflectivity are also included. The experimental results show a maximum around 7.8 eV, while our theory predicts a similar feature around 8.2 eV. The experimental maximum coincides with the critical point in the dielectric function located at 7.8 eV. In addition, the experimental results appear to form a knee at 8.2 eV. The minimum around 9 eV is present in both theory and experiment. The theoretical reflectivity is between the experimental curves for energies smaller than 7.8 eV, but it is higher than experimental values for energies beyond 7.8 eV. Finally, in Fig. 6 we show the calculated values for the refractive index of 3C-SiC. In Fig. 6 we also show available experimental data. The agreement between theory and experiment is very good.

TABLE IV. Calculated and experimental values for the static dielectric constant ϵ_∞.

Theory	Expt.
7.1,[a] 6.95,[b] 7.02,[c] 6.63,[d] 7.33[e]	6.52,[f] 6.7[g]

[a]Present work.
[b]From Ref. 14.
[c]From Refs. 5 and 16.
[d]From Ref. 17.
[e]From Ref. 19.
[f]From Ref. 27.
[g]From Ref. 10.

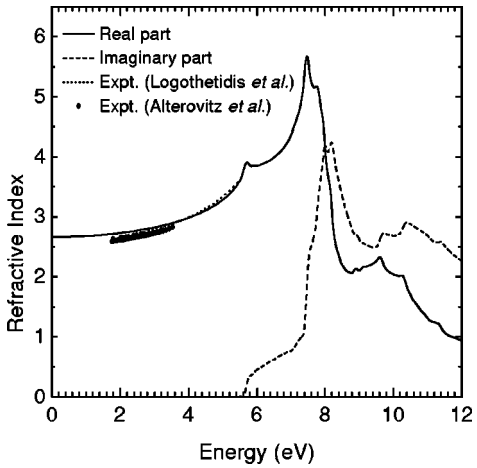

FIG. 6. Calculated real and imaginary part of the refractive index for 3C-SiC. Also shown are the experimental data of Alterovitz *et al.* (Ref. 36) for 10-nμ-thick films, and the data of Logothetidis *et al.* (Ref. 10).

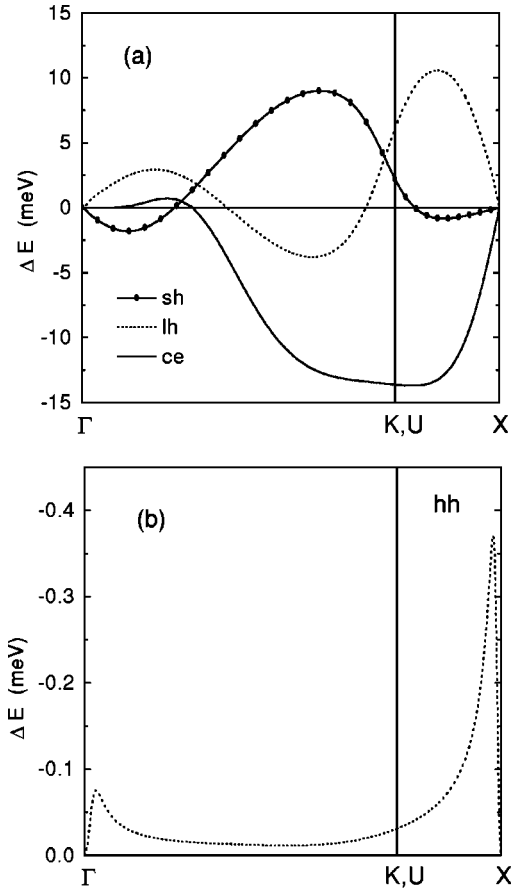

FIG. 7. Spin splitting along the [110] direction of 3C-SiC for (a) the lowest conduction band (ce), the light hole (lh), split hole (sh), and (b) heavy hole (hh) bands.

IV. SPIN SPLITTING

In crystals with inversion symmetry, like the diamond structure, states with different spin orientations are degenerate. In the zinc-blende structure, however, the lack of inversion symmetry may cause splitting of this spin degeneracy; only along $\langle 100 \rangle$ directions all states remain degenerate, while along the $\langle 110 \rangle$ directions the spin degeneracy is removed.[37] In the latter case, states belong to one of the two one-dimensional representations, Σ_3 and Σ_4. The splitting is taken positive if the Σ_4 state is higher in energy than the Σ_3 state. In the calculations, the C atom has been chosen to be at the origin and the Si atom at the position (1/4,1/4,1/4) in units of the lattice constant.

The spin–orbit coupling constants for Si and C are taken equal to[27]

$$\lambda_{\mathrm{Si}} = 15 \ \mathrm{meV}, \quad \text{and} \quad \lambda_{\mathrm{C}} = 2 \ \mathrm{meV}. \tag{7}$$

The results for the spin splitting calculations along the ΓK and UX directions for the lowest conduction electron (ce), heavy hole (hh), light hole (lh), and spin hole (sh) are shown in Fig. 7. We conclude from Fig. 7 that in the entire region the spin splitting for the heavy hole is considerably smaller than for the other bands. In addition, the spin splitting for the conduction electron, close to the Γ point, is very small, even smaller than the splitting for the heavy hole band.

TABLE V. Cubic splitting coefficients γ, (in electron volts times cubic angstrom) for the conduction band electron (ce), the light hole (lh), split hole (sh), and heavy hole (hh) bands. Our calculated values are listed, for comparison, along with those obtained by the LMTO method (Ref. 13).

	γ_{sh}	γ_{lh}	γ_{hh}	γ_{ce}
ETB	−47.9	58.2	−10	0
LMTO[a]	−46.8	54.7	0	−0.54

[a]Ref. 13.

Very close to the Γ point the spin splitting, ΔE, is expanded in terms of k. In the absence of d orbitals, there is no linear term in ΔE and the splitting for small k can be written as[37]

$$\Delta E = \gamma k^3. \tag{8}$$

We use the notation γ_{ce}, γ_{hh}, γ_{lh}, and γ_{sh} to denote splitting for the lowest conduction electron, heavy hole, light hole, and spin hole, respectively. The values obtained using the present ETB model are given in Table V, together with the results from the LMTO method of Ref. 12. There is agreement between these two methods for γ_{lh} and γ_{sh}, while for the value of γ_{hh} the LMTO method gives zero and the ETB model $-10\,\mathrm{eV\,\AA^3}$, and for the value of γ_{ce} the LMTO method gives $-0.54\,\mathrm{eV\,\AA^3}$ and the ETB model zero.

V. CONCLUSIONS

In the present article we have performed calculations for the electronic and optical properties of SiC. For the evaluation of the electronic properties the DFT-LDA method was used, with appropriate corrections to the eigenvalues of conduction states.[25] The calculated band structure gives band gaps in good agreement with GW results. The deformation potentials at the Γ point of the BZ have also been obtained. For the calculation of the optical properties the ETB method was used, which was fitted to reproduce the band structure calculated by the DFT-LDA method. Then the dielectric function was obtained using a fine mesh of $40\times40\times40$ **k** points in the BZ. The critical point structure of the dielectric function was investigated using the second derivative of the dielectric function. The calculated reflectivity has the same structure as the experimental results, with the theoretical values lying between the experimental curves for energies smaller than 7.8 eV, and above those for larger energies. We have noted how experimental results for large energies are quite sensitive to the quality of sample surface. The refractive index was also calculated and the agreement between the calculated refractive index and the available experimental data which cover the region below 5.5 eV is excellent. Finally, the spin splittings along the [110] direction for the three upper valence and the lowest conduction band were calculated.

Our results represent a comprehensive and well converged study of the electronic and optical properties of SiC, improving on existing calculations, and providing the basis for detailed comparison with existing and future experiments. Such comparisons will be useful in studying and identifying bulk phases of this interesting material.

ACKNOWLEDGMENTS

Useful discussions with Professor S. Ves and Professor S. Logothetidis are gratefully acknowledged. The work of one of the authors (G.T.) has been supported in part by the Greek Government Secretariat for Research and Technology, and the work of another author (E.K.) in part by the Foundation for Research and Technology—Hellas (FORTH). The first principles calculations were carried out at the Computational Center of the Physics Department of the University of Crete, Heraklion.

[1] P. A. Ivanov and V. E. Chelnokov, Semicond. Sci. Technol. **7**, 863 (1992).
[2] *Silicon Carbide*, edited by W. J. Choyke, H. Matsunami, and G. Pensl (Akademie, Berlin, 1997), and references therein.
[3] Y. M. Tairov and V. F. Tsvetkov, J. Cryst. Growth **43**, 209 (1978).
[4] J. A. Powell, P. Pirouz, and W. J. Cloyke, in *Semiconductor Interfaces, Microstructures and Devices*, edited by Z. C. Feng (Institute of Physics, Bristol, 1993), p. 257.
[5] B. E. Wheeler, Solid State Commun. **4**, 173 (1966).
[6] W. R. L. Lambrecht, B. Segall, M. Yoganathan, W. Suttrop, R. P. Devaty, W. J. Choyke, J. A. Edmond, J. A. Powell, and M. Alouani, Phys. Rev. B **50**, 10722 (1994).
[7] W. R. Lambrecht, S. Limpijumnong, S. N. Rashkeev, and B. Segall, Phys. Status Solidi B **202**, 5 (1997).
[8] V. I. Gavrilenko, S. I. Florov, and N. I. Klyui, Physica B **185**, 394 (1993), and references therein.
[9] S. Logothetidis, H. M. Polatoglou, J. Petalas, D. Fuchs, and R. L. Johnson, Physica B **185**, 389 (1993).
[10] S. Logothetidis and J. Petalas, J. Appl. Phys. **80**, 1768 (1996).
[11] J. Petalas, S. Logothetidis, M. Gioti, and C. Janowitz, Phys. Status Solidi B **209**, 499 (1998).
[12] M. Rohlfing, P. Krüger, and J. Pollmann, Phys. Rev. B **48**, 17791 (1993).
[13] M. Willatzen, M. Cardona, and N. E. Christensen, Phys. Rev. B **51**, 13150 (1995).
[14] J. Chen, Z. H. Levine, and J. W. Wilkins, Phys. Rev. B **50**, 11514 (1994).
[15] G. Wellenhofer, K. Karch, P. Pavone, U. Rössler, and D. Strauch, Phys. Rev. B **53**, 6071 (1996).
[16] K. Karch, F. Bechstedt, P. Pavone, and D. Strauch, Phys. Rev. B **53**, 13400 (1996).
[17] V. I. Gavrilenko and F. Bechstedt, Phys. Rev. B **55**, 4343 (1997).
[18] B. Adolph, V. I. Gavrilenko, K. Tenelsen, F. Bechstedt, and D. Strauch, Phys. Rev. B **53**, 9797 (1996).
[19] B. Adolph, K. Tenelsen, V. I. Gavrilenko, and F. Bechstedt, Phys. Rev. B **55**, 1422 (1997).
[20] C. Tserbak, H. M. Polatoglou, and G. Theodorou, Phys. Rev. B **47**, 7104 (1993).
[21] P. Hohenberg and W. Kohn, Phys. Rev. **136**, B864 (1964); W. Kohn and L. J. Sham, Phys. Rev. **140**, A1133 (1965).
[22] G. B. Bachelet, D. R. Hamann, and M. Schlüter, Phys. Rev. B **26**, 4199 (1982).
[23] H. J. Monkhorst and J. D. Pack, Phys. Rev. B **13**, 5188 (1976).
[24] See the original work of M. Hybertsen and S. Louie, Phys. Rev. Lett. **55**, 1418 (1985); Phys. Rev. B **34**, 5390 (1986); R. Godby, M. Schlüter, and L. Sham, Phys. Rev. Lett. **56**, 2415 (1986); Phys. Rev. B **37**, 10159 (1988).
[25] L. Fritsche, Physica B **172**, 7 (1991); L. Fritsche, C. Kroner, and T. Reinert, J. Phys. B **25**, 4287 (1992); L. Fritsche, J. Quantum Chem. **48**, 185 (1993); L. Fritsche and Y. M. Gu, Phys. Rev. B **48**, 4250 (1993).
[26] I. N. Remediakis and E. Kaxiras (unpublished).
[27] *Physics of Group IV Elements and III-V Compounds*, Landolt–Börnstein, New Series, Group III, edited by O. Madelung, M. Schulz, and M. Weiss (Springer, Berlin, 1982), Vol. 17, Pt. a.
[28] F. H. Pollak and M. Cardona, Phys. Rev. **172**, 816 (1968).
[29] C. Tserbak and G. Theodorou, Phys. Rev. B **50**, 18179 (1994).
[30] C. Tserbak and G. Theodorou, Phys. Rev. B **52**, 12232 (1995).
[31] F. Wooten, *Optical Properties of Solids* (Academic, New York, 1972).
[32] N. V. Smith, Phys. Rev. B **19**, 5019 (1979).
[33] L. Brey and C. Tejedor, Solid State Commun. **48**, 403 (1983).
[34] O. Jepsen and O. K. Andersen, Solid State Commun. **9**, 1763 (1971).
[35] G. Lehmann and M. Tauc, Phys. Status Solidi B **54**, 469 (1972).
[36] S. A. Alterovitz, J. A. Woollam, in *Handbook of Optical Constants of Solids II*, edited by E. D. Palik (Academic, New York, 1991).
[37] M. Cardona, N. E. Cristensen, and G. Fasol, Phys. Rev. B **38**, 1806 (1988).